Defence Science Journal, Vol. 72, No. 3, May 2022, pp. 334-342, DOI : 10.14429/dsj.72.3.17422

Kinematic Analyses of Metallic Plate Perforation by Penetrators with Various Nose Geometries

T. Akyürek
Çankaya University, Engineering Faculty, Mechanical Engineering Department, 06790 Etimesgut Ankara/Turkey
E-mail: turgutakyurek@cankaya.edu.tr

ABSTRACT

This study analyses kinematics of a metallic plate perforation by a penetrator with truncated ogive nose geometry to find solutions also to blunt, conical, ogive, and hemi-spherical nosed penetrators. Plugging, ductile hole enlargement, dishing, and petal forming failure modes are used in the analyses. Acceleration throughout perforation is calculated by using the related failure mode, analytical model, and the target-penetrator interaction geometry. Depending on the failure model; back lip and front lip formation during ductile hole enlargement, plug formation during plugging, and deflection of target plate during dishing is also analysed. Analyses are based on projectile's equation of motion, momentum and energy equations, and projectile-target plate interactions. The analyses results for selected cases, with the impact velocity range 215-863 m/s, are compared with the test data. The residual velocity estimation for a strike velocity is close to the related test data with an error of 0.3-2.2 %, except for conical nosed penetrators at impact velocities approaching the ballistic limit velocity.

Keywords: Perforation kinematics; Penetrator-plate interaction; Nose geometry; Limit velocity; Terminal ballistics

NOMENCLATURE

A	The displacement of stress wave in radial direction
b	The target plate thickness
c	Velocity of stress wave
c_1	Parameter for static target resistance stress
c_2, c_3	Parameter for dynamic target resistance stress
d_p	Shank diameter of the projectile
D	Flexural rigidity of the target plate per unit width
e_s	Strain energy stored by per unit volume of the target plate
E	Young modulus
E_f	The energy dissipated through friction
E_p	The energy lost by the projectile
E_s	Target plate's strain energy
E_t	Energy absorbed in target
F	The target material resistance to penetration
F_s	Impact force on the target panel
h	Depth of penetration of the penetrator's nose tip at time t
K	Bulk modulus
L	Nose length of the penetrator
L_{eff}	Effective length
m_p	Penetrator's mass
m_{plug}	Plug mass at time t
M_r	Bending moment (radial)
M_q	Bending moment (tangential)
n	Target plate's strain hardening exponent
P_c	The pressure required for cavity expansion
P_0	The required pressure to yield the target plate
Q_r	Shear force per unit length at distance r
R_t	Target's resistance stress to penetration
R_{eff}	Target plate's effective resistance stress
R_t^c	Resistance stress of the target plate under compression
r_c	Cavity radius
r_p	Shank radius of the penetrator
r_{pl}	Plastic zone size
r_r	Distance of penetrator's tip to the target plate's rear surface
r_t	Radius at the truncated nose tip
SCE	Spherical cavity expansion
t	Time
V	The penetrator's instantaneous velocity
V_h	Penetrator's instantaneous velocity at penetration depth h

Received : 17 August 2021, Revised : 09 April 2022
Accepted : 06 May 2022, Online published : 01 July 2022

V_r	Penetrator's residual velocity at the exit of the target plate
V_s	Penetrator's strike velocity
V_0	Limit velocity
v	Volume
ν_h	Volume of penetrator within target when its nose tip is at h
w	Deflection of the target plate in z axis direction
W_p	Work of penetration
x_t	The distance from the un-truncated ogive tip to the truncated tip
Y_t	Target material's strength
ε	Normal strain
ϕ	Nose geometry function
ν	Poisson's ratio (target)
λ,μ	Lame constants
σ	True stress
σ_{eq}	Equivalent stress
σ_y	Target's yield stress
ρ_p	The penetrator's density

1. INTRODUCTION

Objective of the study is to analyse perforation kinematics of metallic target plates at different thicknesses, impacted by the penetrators at different impact velocities, with different masses, and nose geometries, with the intention to obtain acceleration–time, and instantaneous velocity – time graphs for various penetrator-target plate combinations, by studying penetrator nose and target plate interaction, using the appropriate failure mechanisms that require only common test data, and to verify the analytical solutions by using the test data.

Penetration of a plate by a penetrator which has a defined nose profile is studied widely[1]. They are reviewed by the references, such as[2-4]. However, there is a need for a common model that can be applied to the penetrators with various nose geometries.

1.1 Projectile's Equation of Motion

With the assumption of constant cross-sectional area for the penetrator's body, analysis of perforation of target plates by the penetrators can be made by using projectile's equation of motion, as given below[1].

$$\rho_p L_{eff} \frac{dV}{dt} = -R_t = -\left(c_1 + c_2 V + c_3 V^2\right) \tag{1}$$

Eqn (1) yields to Resal equation[5] when c_1=0, and to Poncelet equation[3] when c_2=0.

1.1.1 Resistance to Penetration

Eqn (1) implies that R_t is constant or function of V. R_t is a function of Y_t as R_t=$k_r Y_t$, where k_r is 0.5[6], 0.5 or 1.33[7], 1.92[8], 2.0[9], 3-6[10].

1.1.2 Equation of Motion (Poncelet Equation)

Penetration h can be calculated through integral of Eqn (1) and taking first term of serial expansion of logarithm within limits from V_s to zero[1].

$$\frac{h}{L_{eff}} \cong \frac{\rho_p V_s^2}{2c_1} \tag{2}$$

It is shown that effect of V_s on R_t is negligible also at very thin plates[11].

When h=b, V_s becomes V_0, which can be calculated approximately from Eqn (2) as:

$$V_0 \cong \sqrt{\frac{2c_1 b}{\rho_p L_{eff}}} \tag{3}$$

Using R_{eff}, in place of c_1, as proposed by Rosenberg and Dekel[12] yields to the same energy loss of the projectile. This approach implies that c_2 = 0 and $C_1 = R_{eff}$[1].

1.1.3 Balance of Energy

Energy transfer between penetrator and target could be shown as[13].

$$E_p = E_t = E_S + E_f + W_p \tag{4}$$

E_f could be neglected.

1.1.4 The Strain Energy Stored During Penetration

The stress-strain relationship for elastic and plastic deformation could be written as:

$$\sigma = \begin{cases} E\varepsilon & \text{for } \sigma \le \sigma_y \\ \sigma_y \left(\frac{E\varepsilon}{\sigma_y}\right)^n & \text{for } \sigma > \sigma_y \end{cases} \tag{5}$$

Substituting into the following one would yield to e_s:

$$e_s = \int_0^\varepsilon \sigma d\varepsilon = \int_0^\varepsilon E\varepsilon d\varepsilon + \int_0^\varepsilon \sigma_y \left(\frac{E\varepsilon}{\sigma_y}\right)^n d\varepsilon = \frac{\sigma^2}{2E} + \frac{\sigma_y^{1-n} E^n}{1+n} \varepsilon^{1+n} \tag{6}$$

E_s is found by taking the integral of e_s over the volume.

Equating E_p to the case with V_o, and dividing both sides of the equality with V_o, yields to the following normalised equation.

$$\frac{V_r}{V_0} = \sqrt{\left(\frac{V_s}{V_0}\right)^2 - 1} \tag{7}$$

1.2 Basic Failure Modes

Basic failure modes are briefly explained as follows.

1.2.1 Ductile Hole Enlargement

Ductile hole enlargement is the penetration mode for penetrators with pointed nose if b / d_p > 0.1. SCE theory is widely used in describing ductile hole enlargement. Static SCE modes are analysed by various researchers[14-17]. Bishop *et al.*[14] consider P_c as the required work for generating a cavity of unit volume. P_c is approximately equal to R_t. The following equation for P_c is proposed by Hill[15].

$$P_c = \frac{2}{3} Y_t \left[1 + ln\left(\frac{\mathrm{E}}{3Y_t(1-\nu)}\right)\right] \tag{8}$$

Satapathy[18] proposes the following Eqn to consider thickness effect on P_c:

$$R_t = P_c = \frac{2Y_t}{3}\left[1-\left(\frac{r_{pl}}{r_r}\right)^3\right] - \frac{2}{3}Y_t ln\left[\frac{Y_t}{2\mu}\left\{1+\frac{4\mu}{3\lambda+2\mu}\left(\frac{r_{pl}}{r_r}\right)^3\right\}\right] \quad (9)$$

r_{pl} is calculated as:

$$\frac{r_{pl}}{r_r} = \left[-\frac{Y_t}{6\mu}+\sqrt{\left(\frac{Y_t}{6\mu}\right)^2+\frac{4}{3}\left(\frac{2Y_t}{3}\right)\frac{1}{3\lambda+2\mu}\left(\frac{r_c}{r_r}\right)} \Big/ \left(\frac{4Y_t}{3}\right)\frac{1}{3\lambda+2\mu}\right]^{1/3} \quad (10)$$

r_c is found by using Tate equation[19],

$$\frac{r_c}{r_{pl}} = \sqrt{1+\frac{2\rho_p\left(V_s - V\right)^2}{R_t}} \quad (11)$$

V is calculated by using:

$$Y_p + \frac{1}{2}\rho_p\left(V_s - V\right)^2 = \frac{1}{2}\rho_t V^2 + R_t \quad (12)$$

where $Y_p = 1.7\sigma_p$ and R_t:

$$R_t = \sigma_t\left[\frac{2}{3}+ln\left(0.57\frac{E_t}{\sigma_t}\right)\right] \quad (13)$$

1.2.1.1 Energy Balance

The penetrator's kinetic energy is used for the work of volume change. The energy balance at h:

$$\frac{1}{2}m_p(V_s^2 - V_h{}^2) = R_t^c \Delta v_h \quad (14)$$

V_h is calculated by studying interaction of the penetrator's nose with target plate, as explained in section 2.1. The analysis is based on a truncated (blunt) ogive nosed geometry. Solutions to other nose geometries are obtained from the blunt ogive analysis.

1.2.2 Plugging

The references[20-21] provide basic theory on plugging. Plugging usually occurs when V_s is close to V_0[10].

Conservation of momentum for the plug attached to the penetrator:

$$m_p V_s = \left(m_p + m_{plug}\right)V_r \quad (15)$$

Conservation of energy, with the assumption of adiabatic process, can be written as:

$$\frac{1}{2}m_p V_s^2 = \frac{1}{2}\left(m_p + m_{plug}\right)V_r^2 + W_p + E_s \quad (16)$$

When $V_s = V_0$, $V_r = 0$, $W_p = m_p V_0^2/2$. Substituting these values into Eqn (16) and neglecting E_s results in[10]:

$$\frac{V_r}{V_0} = \sqrt{\frac{1}{1+m_{plug}/m_p}}\sqrt{\frac{V_s^2}{V_0^2}-1} \quad (17)$$

For the blunt nosed penetrators, Eqn (17) takes the form:

$$\frac{V_r}{V_0} = \frac{1}{1+m_{plug}/m_p}\sqrt{\frac{V_s^2}{V_0^2}-1} \quad (18)$$

For thin plates ($b \le 2r_p$), Eqns (17) and (18) convert to Eqn (7) if $m_{plug} = 0$.

1.2.3 Dishing

Dishing, analysed by Woodward and Cimporeu[22], is due to stretching and bending of the plate around the impact point. Impact creates stress waves with velocity c, and imposes a transverse F_s on the target, which is equal to R_t. Figure 1 shows the internal loads at r from the strike point.

Q_r is calculated for a clamped-edge circular plate as[1]:

$$Q_r = \mathrm{D}\frac{\mathrm{d}}{dr}\left(\frac{d^2w}{dr^2}+\frac{1}{r}\frac{dw}{dr}-r^2\right) = \frac{F_s}{2\pi r} \quad (19)$$

$$\frac{\mathrm{d}}{dr}\left[\frac{1}{r}\frac{d}{dr}\left(r\frac{dw}{dr}\right)\right] = \frac{Q_r}{D} \quad (20)$$

where D is:

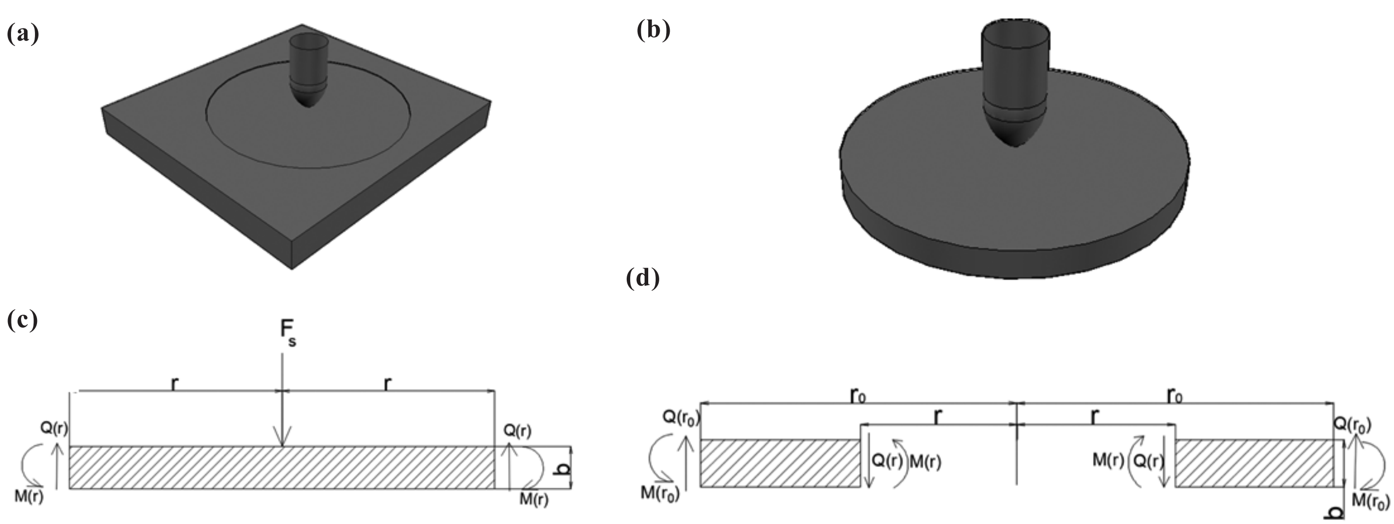

Figure 1. Penetrator's impact at a panel: (a) Overall view, (b) Stressed region, (c) Internal loads at r, (d) Internal loads at r_0[1].

$$\mathrm{D} = \frac{\mathrm{E}b^3}{12\left(1-\nu^2\right)} \tag{21}$$

c is calculated as

$$c = \sqrt{\frac{K}{\rho_t}} = \sqrt{\frac{E}{3\left(1-2\nu\right)}\frac{1}{\rho_t}} \tag{22}$$

Ballistic design requires high specific stiffness to transmit stress wave far from the impact point[23].

The deflection w is calculated as follows by using Eqns (19) & (20):

$$w = \frac{F_s}{16\pi D}\left(2r^2 ln\frac{r}{a} + a^2 - r^2\right) \tag{23}$$

Where $a = ct$. w is maximum at $r=0$:

$$w_{max} = \frac{F_s \mathrm{a}^2}{16\pi D} \tag{24}$$

M_r and M_θ are found to be:

$$M_r = \mathrm{D}\left(\frac{d^2w}{dr^2} + \frac{\nu}{r}\frac{dw}{dr}\right) = \frac{F_s}{4\pi}\left[1 + \left(1+\nu\right)ln\frac{r}{a}\right] \tag{25}$$

$$M_\theta = \mathrm{D}\left(\nu\frac{d^2w}{dr^2} + \frac{1}{r}\frac{dw}{dr}\right) = \frac{F_s}{4\pi}\left[\nu + \left(1+\nu\right)ln\frac{r}{a}\right] \tag{26}$$

M_r and M_θ at $r=0$ could be found as[24]:

$$M_r = M_\theta = \frac{F_s}{4\pi}\left[\left(1+\nu\right)ln\frac{a}{0.325b}\right] \tag{27}$$

The stresses at $r=0$:

$$\sigma_{rr} = \sigma_{\theta\theta} = -\frac{12\mathrm{z}}{b^3}M = -\frac{3zF_s}{\pi b^3}\left[\left(1+\nu\right)ln\frac{a}{0.325b}\right] \tag{28}$$

The bending stress is maximum at $r=0$:

$$\sigma_{rr}^{max} = \sigma_{\theta\theta}^{max} = -\frac{6}{b^2}M = -\frac{3F_s}{2\pi b^2}\left[\left(1+\nu\right)ln\frac{a}{0.325b}\right] \tag{29}$$

F_s is found by equating E_s to projectile's kinetic energy at V_0:

$$E_p = E_t = E_s + W_p = \frac{1}{2}m_p V_0^2 = \frac{1}{2}F_s w_{max} = \frac{F_s^2 a^2}{32D} \tag{30}$$

$$F_s = \sqrt{\frac{16Dm_pV_0^2}{a^2}} = \frac{V_0}{a}\sqrt{\frac{4Eb^3m_p}{3\left(1-\nu^2\right)}} \tag{31}$$

1.2.4 Petal Formation

Petal formation is observed with sharp-nosed projectiles when $b / d_p < 0.1$. It occurs when σ_{rr} and $\sigma_{\theta\theta}$ reach R_t, and V_s is close to V_0.

2. METHODOLOGY

Kinematics of plate perforation by a penetrator with blunt ogive nose is analysed to find solutions to the penetrators with all common nose geometries such as ogive, hemi-spherical, conical, and blunt. Acceleration and velocity histories during perforation are obtained by first deciding on the failure mode, and then using the related analytical model and the penetrator-target plate interaction geometry.

2.1 Analyses of Perforation

2.1.1 Blunt Ogive Nosed Penetrator

Perforation through hole enlargement or plugging of a target plate by a truncated ogive projectile is idealized and schematically shown in Fig. 2, with the four cases that might occur: 1) $h< b$ and L, 2) b<h<L, 3) $h>b$ and L, 4) L<h<b. There

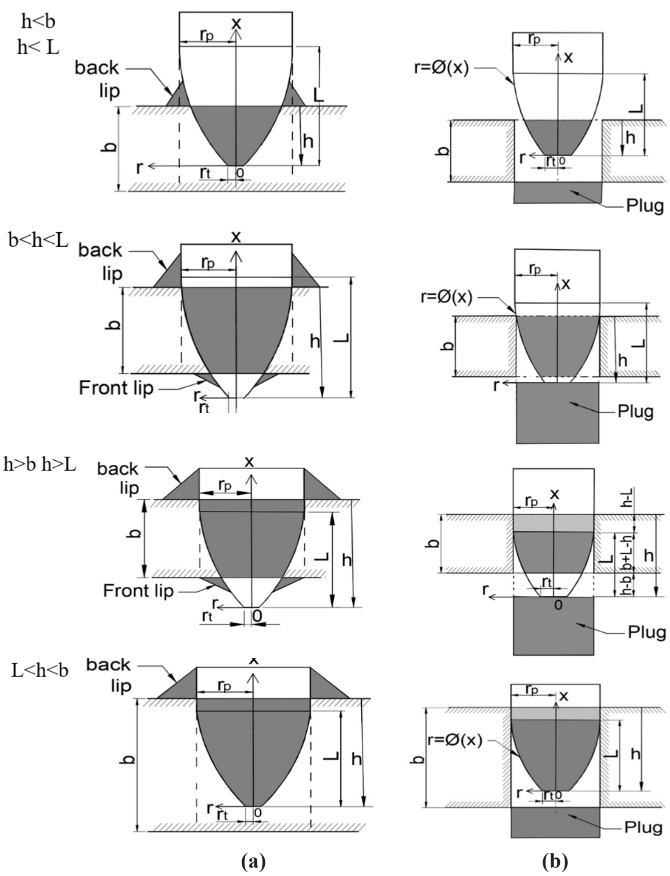

Figure 2. Schematic illustration of perforation phases in: (a) Hole enlargement, (b) Plugging.

are two coordinate systems: a system moving with impactor (r and x), and a fixed system (h)[25]. During hole enlargement, lips are created, whose volume is assumed to be equal to the volume swept by the projectile. First, the back lip is observed, and its volume increases till h reaches b. Then, the front lip emerges and enlarges with increasing h.

Nose profile of the impactor is written as follows, with the coordinate origin at the nose tip:

$$r = \varnothing\left(x\right) = \sqrt{r_o^2 - \left(L-x\right)^2} + r_p - r_o \tag{32}$$

$$r_o = \frac{r_p^2 + \left(L + x_t\right)^2}{2r_p} \tag{33}$$

where x_t is found as:

$$x_t = L - \sqrt{2r_o\left(r_p + r_t\right) - \left(r_p - r_t\right)^2} \tag{34}$$

Assuming that the penetrator is rigid, the penetration will create a displacement of target's material, whose displaced volume is equal to the penetration volume of the penetrator into the target. The displaced volume due to differential penetration depth (dh) is:

$$dv = \pi\phi^2(h)dh = \pi\left(\sqrt{r_o^2 - (L-h)^2} + r_p - r_o\right)^2 if\ h \le L \tag{35}$$

Integration of Eqn (35) will give the total amount of displaced volume (Δv_h)) at h. For the case $h \le b,\ h \le L$, Δv_h is calculated as:

$$\Delta v_h = \int_{h=0}^{h} \pi\left(\sqrt{r_o^2 - (L-h)^2} + r_p - r_o\right)^2 dh = \pi(A+B+C) \tag{36}$$

$$A = h\left[r_o^2 - L^2 + h\left(L - \frac{h}{3}\right)\right] \tag{37}$$

$$B = \left(r_p - r_o\right)\left[(h-L)\sqrt{r_o^2-(L-h)^2} + r_o^2 tan^{-1}\left(\frac{h-L}{\sqrt{r_o^2-(L-h)^2}}\right)\right] + \left(r_p - r_o\right)\left[L\sqrt{r_o^2 - L^2} - r_o^2 tan^{-1}\left(\frac{-L}{\sqrt{r_o^2 - L^2}}\right)\right] \tag{38}$$

$$C = h\left(r_p - r_o\right)^2 \tag{39}$$

Δv_h for b<h<L:

$$\Delta v_h = \int_{h=h-b}^{h} \pi\left(\sqrt{r_o^2 - (L-h)^2} + r_p - r_o\right)^2 dh = \pi(A+B+C) \tag{40}$$

A, B and *C* values in Eqn (40) are calculated by substituting the related limit values. Δv_h for $h>b$ and L:

$$\Delta v_h = \int_{h=h-b}^{L} \pi\left(\sqrt{r_o^2 - (L-h)^2} + r_p - r_o\right)^2 dh + \pi r_p^2(h-L) = \pi(A+B+C) + \pi r_p^2(h-L) \tag{41}$$

A, B and *C* values in Eqn (41) are calculated by substituting the related limit values.

For $L<h<b$, *A, B, C* values are found by using the limit values from h-L to h.

V_h can be found from Eqn (14) as:

$$V_h = \sqrt{\frac{m_p V_s^2 - 2Y_t^c \Delta v_h}{m_p}} \tag{42}$$

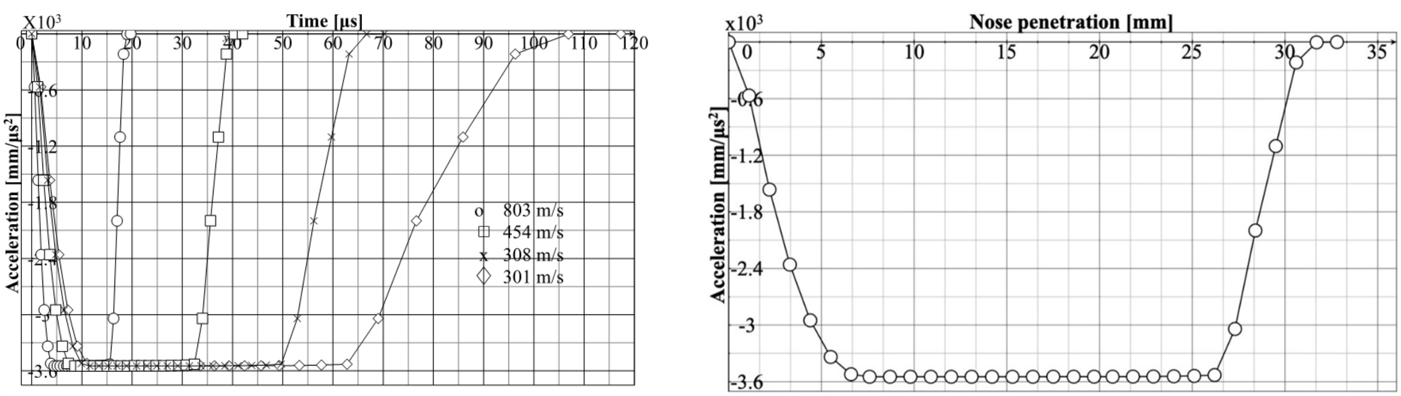

(a) (b)

Figure 3. Acceleration variation with; (a) Perforation time and (b) Nose penetration.

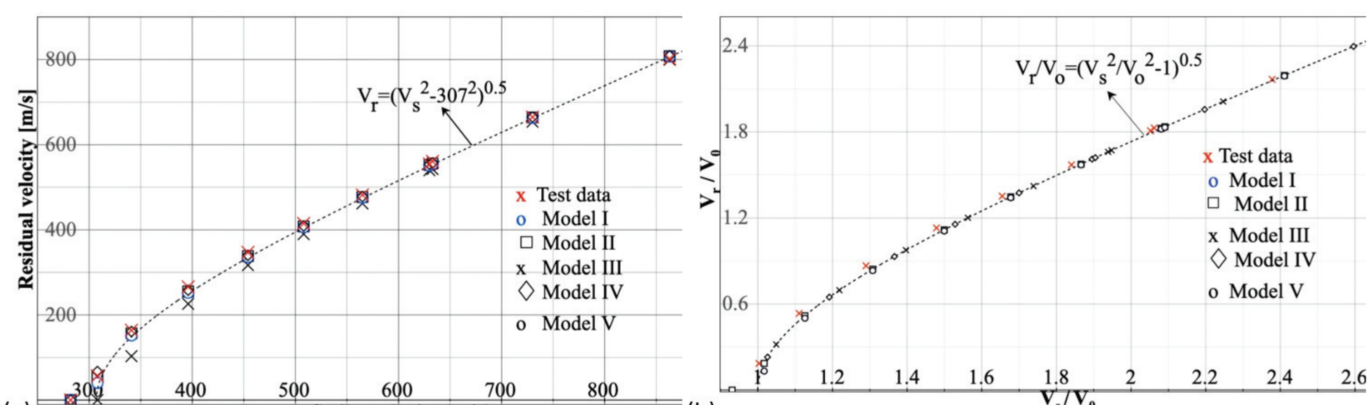

(a) (b)

Figure 4. $V_r - V_s$ comparison charts: (a) Values and (b) Normalized values.

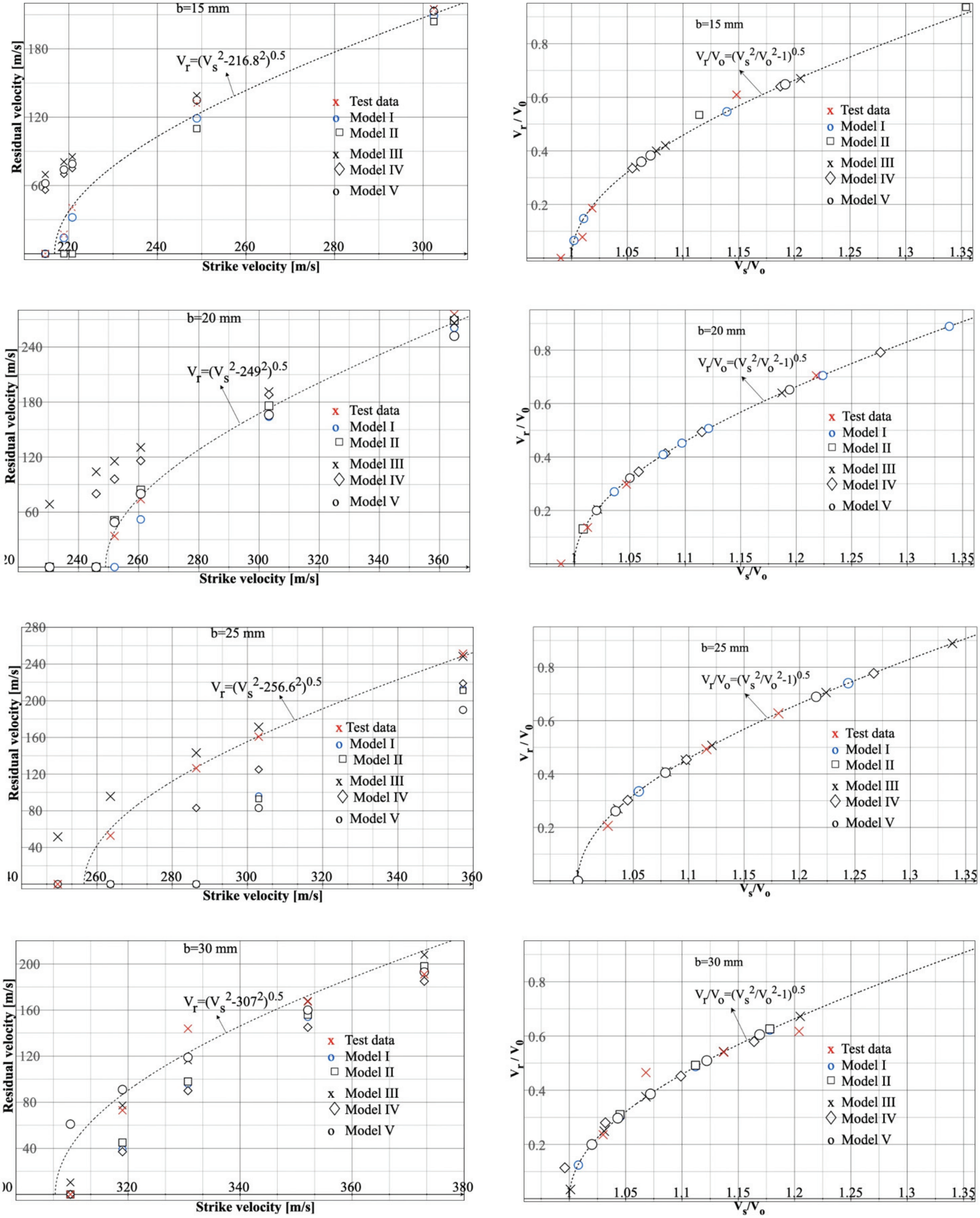

(a) (b)

Figure 5. ***Vr - Vs*** **comparison charts for different thicknesses: (a) Values, (b) Normalized values.**

V_r is calculated by substituting b for h in Eqn (42) as:

$$V_r = \sqrt{\frac{m_p V_s^2 - 2Y_t^c \Delta v_b}{m_p}} \tag{43}$$

V_o can be found from Eqn (43) as:

$$V_0 = \sqrt{\frac{2Y_t^c \Delta v_b}{m_p}} \tag{44}$$

2.1.2 Ogive Nosed Penetrator

When replacing x with $(x' - x_t)$ and L with $(L' - x_t)$, coordinate system origin moves to the tip of un-truncated nose location. Then, substituting $x_t = 0$ and $r_t = 0$ in the equations of truncated ogive geometry, yield to the solutions for the un-truncated.

2.1.3 Hemi-Spherical Nosed Penetrator

By replacing r_0 and L' with r_p, the solutions for ogive nose result in with the ones for hemispherical nose. Penetration mode might change from adiabatic shear plugging to ductile hole enlargement.

2.1.4 Conical Nosed Penetrator

By replacing $A + B + C$ with $\pi r_p h^3 / (3L')$, solutions for ogive-nosed projectile result in with the ones for conical nose.

2.1.5 Blunt Nosed Penetrator

By taking $r_t = r_p, r_0 = r_p, x' = L', x_t = L' = r_p, L = 0$, solutions for ogive-nosed penetrator result in with the ones for blunt nose.

2.2 Penetration Mode

Five models were used in analysing kinematics of perforation. SCE mode, adapted for finite thickness, is used in *Model I*. *Model II* is like *Model I* but with Hill's *SCE* theory. *Model III* uses plastic flow theory based on momentum and energy conservation. *Model IV* is an energy and momentum based plugging theory. *Model V* is the parametric model proposed by Forrestal *et al.*[26].

3. RESULTS AND DISCUSSION

Kinematic analyses were done for three different cases, with the test data from literature, by applying the theories put forward here.

3.1 Test Case I

The test data from the literature[27] is on the steel projectiles with ogive nose that were impacted at the 26.3 mm thick - 6061-T651 aluminium plate with various V_s values.

Acceleration versus perforation time and nose tip penetration through the target thickness at various strike velocities are analysed with the selected models. As an example, the results with *Model I* are shown in Fig. 3.

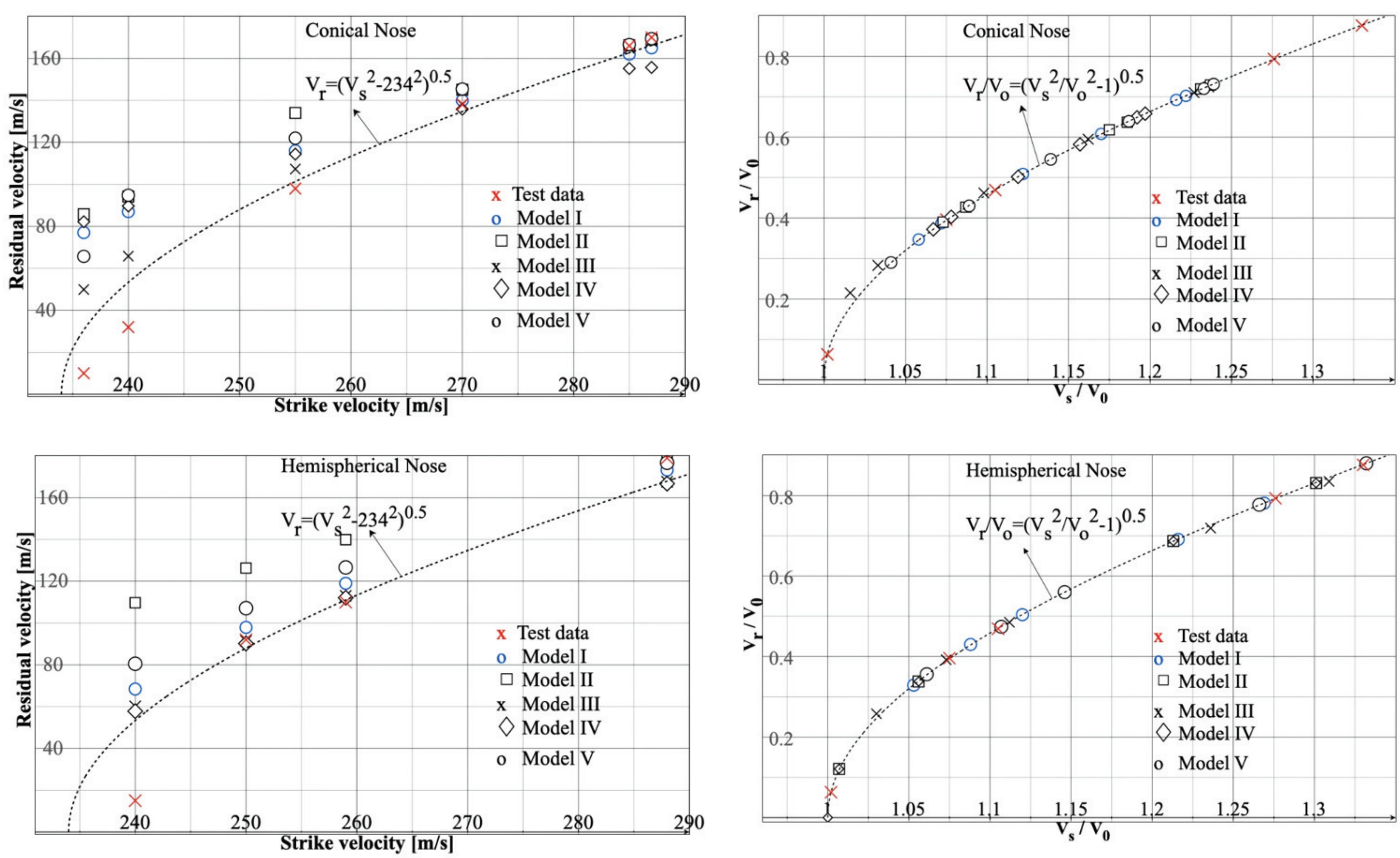

(a) (b)

Figure 6. *Vr - Vs* comparison charts for different nose geometries: (a) Values, (b) Normalized value.

V_r - V_s graph with the values calculated by using different models, and test data are shown in Fig. 4.

V_r - V_s calculations are in line with the test data. The normalized velocity values perfectly fit into the idealized Recht - Ipson curve[28]. Residual velocity predictions with Model I and V are with an error of 0.3-2.2 % for all velocities. Model II predicts the results with good estimations. Model III underestimates V_r. The best calculations are with Model IV.

3.2 Test Case II

The test data from the literature[29] is on conical nosed steel penetrators impacting at the AA5083-H116 aluminium plates of thickness 15-30 mm with various V_s values.

V_r - V_s graphs with the values calculated for different thicknesses by using different models, and the test data are shown in Fig. 5.

V_r - V_s calculations are in line with the test data at high strike velocities at all target plate thicknesses except for 25 mm, for which the test data do not seem to be in line with the other thicknesses of the same material. For b=15 mm, Model I estimations are the best. For b=20 mm, the results with Models II and *V* are good. For b=30 mm, Model III results are the best.

3.3 Test Case III

The test data from the literature[30] is on conical, blunt, or hemispherical nosed stell projectiles that are impacted at the 3 mm thick Mars 300 steel plates with various V_s values.

Residual velocity graphs that provide test data and calculations comparison are given in Fig. 6. For blunt nosed penetrators, all models except III and V predict the results in good agreement with the test data. For projectiles with conical nose, Models III, V, and I results are good at all velocities except the ones approaching V_o. In the case of projectiles having hemispherical nose, Models III, IV and I estimations are good at all velocities.

4. CONCLUSIONS

Analyses of plate perforation by a truncated ogive nosed penetrator provide solutions also to the penetrators with common nose geometries such as ogive, hemispherical, conical, and blunt.

Kinematic analyses have been made with various test cases that are available in the literature[28-30.] V_r - V_s calculations are in line with the test data for most of the models used. In general, estimations are good at the velocities not approaching V_0.

REFERENCES

1. Akyürek, T. Analyses of plate perforation for various penetrator-target plate combinations, *J. Mech. Sci. Technol.*, 2022, **36**(4), 1749-1760.
   doi: 10.1007/s12206-022-0311-7
2. Ben-Dor, G.; Elperin, T. & Dubinsky, A. Analytical engineering models of high speed normal impact by hard projectiles on metal shields. *Central Eu. J. Eng.,* 2013, **3**(3), 349-373.
   doi: 10.2478/s13531-013-0108-7
3. Anderson, C.E. Analytical models for penetration mechanics: A review. *Int. J. Impact Eng.,* 2017, **108**, 3-26.
   doi: 10.1016/j.ijimpeng.2017.03.018
4. M.E. Backman, M.E. & Goldsmith, W. The mechanics of penetration of projectiles into targets. *Int. J. Eng. Sci.,* 1978, **16**(1), 1-99.
5. Buchely, M. & Maranon, A. Spherical cavity expansion approach for the study of rigid-penetrator's impact problems. *Applied Mechanics,* 2020, **1**, 20-46.
   doi: 10.3390/applmech1010003
6. Sodha, M.S. & Jain, V.K. On physics of armor penetration. *J. Appl. Physics,* 1958, **29**(12), 1769-1770.
   doi: 10.1063/1.1723044
7. Taylor, G.I. The formation and enlargement of a circular hole in a thin plastic plate, *Q. J. Mech. Appl. Mat.,* 1948, **1**, 103-124.
   doi: 10.1093/qjmam/1.1.103
8. Hill, R. A theory of the plastic bulging of a metal diaphragm by lateral pressure, *Philosophical Magazine,* 1950, **41** (322), 1133-1142.
   doi: 10.1080/14786445008561154
9. Bethe, H.A. An attempt at a theory of an armor penetration, Ordnance Lab. Rep., Frankford Arsenal, 1941.
10. Rosenberg, Z. & Dekel, E. Terminal ballistics, Springer, Singapore, 2016. 359 p.
    doi: 10.1007/978-981-10-0395-0
11. Bhure, V.; Tiwari, G.; Iqbal, M.A. & Gupta, P.K. The Effect of target thickness on ballistic resistance of thin aluminum plates. In Proc. of Int. Symp. on Functional Mater. (ISFM-2018): Energy and Biomed. Applications, 2018.
    doi: 10.1016/j.matpr.2020.01.317
12. Rosenberg, Z. & Dekel, E. Revisiting the perforation of ductile plates by sharp-nosed rigid projectiles. *Int. J. Solids Structures,* 2010, **47**, 238-250.
    doi: 10.1016/j.ijsolstr.2010.07.003
13. Xu, Y. Stabbing resistance of soft ballistic body armor impregnated with shear thickening fluid, University of Manchester, Manchester, UK, 2016. (PhD Thesis).
14. Bishop, R.F.; Hill, R. & Mott, N.F. The theory of indentation and hardness tests, *The Proc. Physical Soc.,* 1945, **57**(3), 147-159.
    doi: 10.1088/0959-5309/57/3/301
15. Hill, R. The mathematical theory of plasticity, Oxford University Press, UK, 1950. 350 p.
16. Hopkins, H.G. Dynamic expansion of spherical cavities in metal, *In* Progress in solid mechanics, edited by I. N. Sneddon & R. Hill, North- Holland Publishing Co., Amsterdam, NL, 1960. Chapter III.
17. Luk, V.K.; Forrestal, M.J. & Amos, D.E. Dynamic spherical cavity expansion of strain-hardening materials. *J. Appl. Mechanics,* 1991, **58**(1), 1-6.
    doi: 10.1115/1.2897150
18. Satapathy, S. Application of cavity expansion analysis to penetration problems, The University of Texas at Austin, Austin, Rep. No: IAT R 0136, July 1997.
19. Tate, A. Long rod penetration methods - Part II. Extensions

to the hydrodynamic theory of penetration. *Int. J. Eng. Sci.,* 1986, **28**(9), 599-612.
20. Wen, H.M. & Sun, W.H. Transition of plugging failure modes for ductile metal plates under impact by flat-nosed projectiles. *Mech. Based Design Struct. Mach.,* 2010, **38**, 86-104.
doi: 10.1080/15397730903415892
21. Pasquali, M. & Gaudenzi, P. Analytical prediction of high-velocity impact resistance of plane and curved thin composite targets. *Aerotecnica Missili Spazio,* 2019, **98**, 111-118.
doi: 10.1007/s42496-019-00011-8
22. Woodward, R.L. & Cimporeu, S. A study of the perforation of aluminum laminate targets. *Int. J. Impact Eng.,* 1998, **21**(13), 117-131.
doi: 10.1016/S0734-743X(97)00034-1
23. Saint, B. The manufacturing and ballistic testing of tri-axial quasi three-dimensional woven composites layered in polyurea, The University of Mississippi, Mississippi. US, 2013. (MS Thesis)
24. Sun, Q.P. https://mae.hkust.edu.hk/~meqpsun/Notes/Chapter3.pdf. (Accessed on 02.09.2021).
25. Ben-Dor, G.; Dubinsky, A. & Elperin, T. Applied high-speed plate penetration dynamics, Springer, 2006.
26. Forrestal, M.J. & Warren, T.L. Penetration equations for ogive-nose rods into aluminum targets. *Int. J. Impact Eng.,* 2008, **35**, 727-730.
doi: 10.1016/j.ijimpeng.2007.11.002
27. Piekutowski, A.J.; Forrestal, M.J.; Poormon, K.L. & Warren, T.L. Perforation of aluminum plates with ogive-nose steel rods at normal and oblique impacts. *Int. J. Impact Eng.,* 1996, **18**(7-8), 877-887.
doi: 10.1016/S0734-743X(96)00011-5
28. Recht, R. & Ipson, T.W. Ballistic perforation dynamics. *J. Appl. Mech.,* 1963, **30**, 384-390.
doi: 10.1115/1.3636566
29. Borvik, T.; Arild, H.C.; Hopperstad, O.S. & Magnus, L. Perforation of AA5083-H116 aluminum plates with conical-nose steel projectiles-experimental study. *Int. J. Impact Eng.,* 2004, **30**, 367-384.
doi: 10.1016/S0734-743X(03)00072-1
30. Teresa, F.; Roth, C. & Mohr, D. Dynamic perforation of ultra-hard high strength armor steel: Impact experiments and modeling.” *Int. J. Impact Eng.,* 2019, **131**, 256-271.
doi: 10.1016/j.ijimpeng.2019.05.008

CONTRIBUTOR

Dr T. Akyürek is Asst. Prof. in Mechanical Engineering Department of Çankaya University, Ankara, Turkey. He received his PhD in Mechanical Engineering from Middle East Technical University, Ankara, Turkey. His research interests include: Impact mechanics, crash tests and crashworthiness, fracture mechanics, terminal ballistics, fatigue, damage tolerance, macro and micro analysis of composites, and design of composite structures.